Analytical Model of Axisymmetric Afterbody Flow Separation

Walter M. Presz Jr.*
Pratt & Whitney Aircraft, East Hartford, Conn.
and
Edward. T. Pitkin†
University of Connecticut, Storrs, Conn.

A practical engineering approach to the prediction of pressure distribution and boundary layer separation point location on afterbodies in subsonic flow is developed. Experimental data are reviewed and the inadequacy of currently available separation prediction methods is demonstrated. A control volume technique is developed as an alternative and is shown to have merit. The separation bubble is then modeled and another control volume technique is developed to predict its outer boundary. Finally, these two developments are combined with a conventional inviscid flowfield calculation and a boundary-layer analysis to produce an iterative procedure to predict pressure distribution and separation point location on an afterbody given only body shape and freestream flow condition.

Introduction

BOUNDARY-layer flow separation often occurs on the aft-end of a multi-mission aircraft resulting in an increase in aircraft drag and a decrease in jet engine performance. Separation occurs in these areas because of the large adverse pressure gradients coupled with thick boundary layers that often exist on the aircraft afterbody. Figure 1 schematically represents the type of flowfield that results. A solid surface sting is used to represent the exhaust jet both analytically and experimentally. The use of the sting is a simplification that eliminates additional variables that affect plume shape and plume entrainment of the afterbody flowfield. This model also possesses a measurable reattachment point for the separated recirculation region as shown in Fig. 1.

Most available techniques for predicting separation use only attached boundary layer and inviscid flow pressure distribution calculations to predict the occurrence of separation. This approach is inherently limited because separation and the resultant recirculation region can drastically alter the afterbody pressure distribution which can in turn significantly alter the position of the separation point. This limitation, as well as a paucity of useful experimental data, motivated the authors to conduct a detailed experimental and analytical program of flow separation over axisymmetric afterbody models.

The recently published[1,6] results of the experimental program represent a systematic data set where the separation pressure environment as well as location and extent of the separation region were measured. The models include circular arc, elliptic, and conical afterbody shapes with mean angles of 8°, 16°, and 24°. More detailed information on the model shapes can be obtained from Ref. 6. The testing was conducted in a blowdown tunnel having a model blockage ratio of about 8%. This blockage effect was subsequently included in all the analytical pressure predictions reported here. The object of the test program was to experimentally locate regions of separation on an afterbody while simultaneously measuring the pressure environment causing the separation in order to provide consistent data for developing an analytical separation model. The measured separation position was found to be a strong function of afterbody shape and freestream Mach number, and a weak function of Reynolds number and approach boundary layer properties. Several commonly used separation criteria were applied to the test flow fields with large discrepancies resulting between the analyses and data as shown in Fig. 2 which is typical.[6] This figure presents results for an elliptical afterbody with a 16° mean angle (β) at a freestream Mach number of $M=0.7$. A "shape factor" separation criterion[2] and Goldschmied's[3] criterion predict no separation. On the other hand, Page's[5] criterion predicts separation on the downstream sting while Stratford's[4] criterion predicts separation much too late. These results show clearly that most commonly used separation criteria are unreliable for predicting the point of separation on axisymmetric afterbodies. An interesting and typical characteristic of this interaction between the separated region and the inviscid flowfield is the plateau pressure distribution readily evident in Fig. 2. This could not be predicted with conventional techniques available at the time this program was started. As shown in Ref. 1, it was found that the separated recirculation region effects upon the inviscid flowfield and afterbody surface pressures could be modeled fairly well by a conical dividing streamline surface placed between the points of separation and reattachment. With these results in hand, an engineering analysis was developed for predicting the pressure distribution on an afterbody in the absence of experimental data.

Discussion

The engineering analysis developed is iterative in nature and combines four major flowfield components: the inviscid flowfield; the attached boundary layer; the point of separation; and the separated recirculating flow region. It was found that the attached boundary layer and inviscid flow can be calculated quite accurately using existing techniques. However, the point of separation and the separated reverse flow region required further consideration before the above

Presented as Paper 75-65 at the AIAA 13th Aerospace Sciences Meeting, Pasadena, Calif., January 20-22, 1975; submitted February 27, 1975; revision received October 29, 1975. The computational part of this work was performed in the computer center of the University of Connecticut, which is supported in part by Grant GJ-9 of the National Science Foundation.

Index categories: Aircraft Aerodynamics (including Component Aerodynamics); Jets, Wakes, and Viscid-Inviscid Flow Interactions; Airbreathing Propulsion, Subsonic and Supersonic.

*Assistant Project Engineering, Propulsion Integration Group. Associate Member AIAA.

†Professor of Mechanical and Aerospace Engineering. Associate Fellow AIAA.

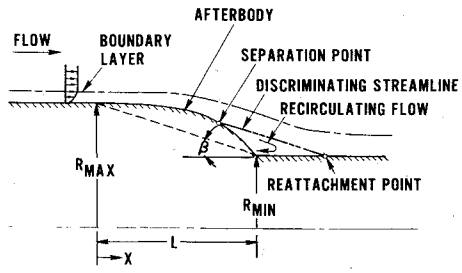

Fig. 1 Schematic of a separated afterbody flowfield.

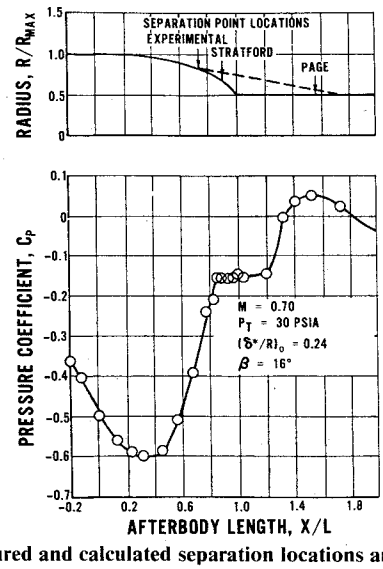

Fig. 2 Measured and calculated separation locations and corresponding pressures on an elliptical afterbody.

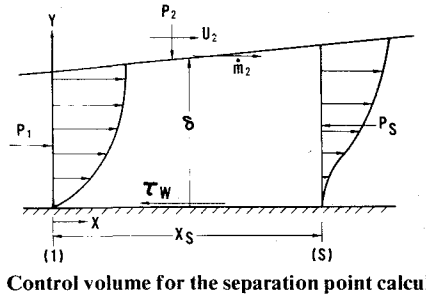

Fig. 3 Control volume for the separation point calculation.

approach could be taken. The following sections summarize the work accomplished in each of these two respective areas.

Separation Point Prediction

Tyler and Shapiro[7] presented an analysis for the pressure rise required for separation in an interaction between a turbulent boundary layer and shock wave. A momentum equation for the control volume, the ideal gas equation of state, the energy equation for isoenergetic flow, the continuity equation for control volume, and the isentropic relations were used to solve for a separation pressure. In its original form, this approach gave poor comparison with data for afterbody separation mainly because of a poorly modeled velocity profile at separation. This analysis was therefore combined with the compressible law of the wall-law of the wake velocity profile.[8] The resulting analysis was quite accurate for predicting separation point location on afterbody shapes, and thus, was further developed and chosen as our separation point criteria. The next two paragraphs will outline the improved calculation procedure for two-dimensional flow on an afterbody.

A control volume is located between the minimum pressure station, designated 1, and the separation point, designated s, in Fig. 3. The wall and outer edge of the boundary layer form the remaining boundaries of the control volume. The length of the control volume is relatively short since separation is known to follow closely after the minimum pressure point on an afterbody. The continuity and momentum equations for the control volume can then be written as

$$\int_0^{\delta_1} (\rho u)_1 dy + \dot{m}_2 = \int_0^{\delta_s} (\rho u)_s dy \tag{1}$$

$$(P\delta)_1 + \int_0^{\delta_1} (\rho u^2)_1 dy + \dot{I}_2 + P_2((\delta_s - \delta_1)$$

$$= \tau_w x_s + (P\delta)_s + \int_0^{\delta_s} (\rho u^2)_s dy \tag{2}$$

where

$$P_2 \triangleq \frac{1}{X_s}\int_0^{X_s} P dX, \quad \tau_w \triangleq \frac{1}{X_s}\int_0^{X_s} \tau dX$$

and where $\dot{I}_2$ is the x-momentum associated with the entrainment mass, $\dot{m}_2$. Introducing the equation of state and the definitions of Mach number and displacement thickness, the continuity equation in integrated form becomes

$$\frac{\delta_1}{\delta_s} = \frac{P_s M_s (2+(\gamma-1)M_s^2)^{1/2}(1-\delta^*/\delta)_s}{(1+\dot{m}_2/\dot{m}_1)P_1 M_1 (2+(\gamma-1)M_1^2)^{1/2}(1-\delta^*/\delta)_1} \tag{3}$$

The momentum equation in integrated form becomes

$$\frac{\delta_1}{\delta_s} = \frac{\dfrac{P_2-P_s}{P_1} - \gamma M_s^2 \dfrac{P_s}{P_1}\left(1-\dfrac{\delta^*}{\delta}-\dfrac{\theta}{\delta}\right)_s}{\dfrac{P_2}{P_1} - 1 - \gamma M_1^2\left(1-\dfrac{\delta^*}{\delta}-\dfrac{\theta}{\delta}\right)_1 - \dfrac{\dot{I}_2}{P_1\delta_1} + \dfrac{\tau_w x_s}{P_1\delta_1}} \tag{4}$$

The entrainment rate is calculated using a relation due to Green.[9]

$$\dot{m}_2 = 0.03(\rho u)_2 X_s [(\delta_1 - \delta_1^*)/\theta_1 - 3]^{-.62} \tag{5}$$

The functional form of this equation was obtained by Green using the velocity defect law[10] for turbulent boundary layers while the constants were obtained empirically. This entrainment equation has been shown to give good agreement with boundary layer flows in zero pressure gradient and in flows proceeding to separation.[11] The corresponding entrained momentum is then

$$\frac{\dot{I}_2}{P_1\delta_1} = \frac{\dot{m}_2}{\dot{m}_1}\left(1-\frac{\delta^*}{\delta}\right)_1 \gamma M_1 M_2 \left(\frac{2+(\gamma-1)M_1^2}{2+(\gamma-1)M_2^2}\right)^{1/2} \tag{6}$$

The continuity and momentum Eqs. (3) and (4) are the two basic equations for the problem, and the two unknowns are P_s and δ_s. Equating the two relations eliminates δ_s leaving an implicit relation for P_s. A boundary layer velocity profile at separation, x_s, must be assumed before a solution is possible. Mathews'[12] compressible version of Coles' law of the wall-law of the wake with $C_f = 0$ to simulate the velocity profile at the separation point was selected. The resulting profile is

$$\left(\frac{u}{u_e}\right)_s = E^{+.5}\sin[.5\sin^{-1}(E^{-.5})(1-\cos(\pi y/\delta_s))] \tag{7}$$

where

$$E = [1+2/[(\gamma-1)M_s^2] \tag{8}$$

so the nondimensional profile is a function of Mach number only. If the separation Mach number, M_s, is known, the ratios $(\delta^*/\delta)_s$ and $(\theta/\delta)_s$ appearing in Eqs. (3) and (4) can then be easily evaluated. If the external pressure distribution $P(x)$ is given, one can obtain x_s from $P(x_s)$, while M_s is obtainable from P_s through isentropic relations. Thus, the separation point location can be calculated directly from the conservation equations. In this separation point prediction model, the normal pressure field and boundary-layer streamline curvature associated with the wall curvature are assumed unimportant in accordance with the standard boundary layer assumption that the flow is essentially similar to that on a flat plate with the same pressure gradient imposed. The separation point velocity profile used in this analysis is also linked to this assumption since it was originally developed for a flat wall with a pressure gradient superimposed.

This separation point prediction scheme was used with the measured boundary layer characteristics and pressure distribution taken from Ref. 6 to predict the separation point locations on several afterbodies. Figures 4 and 5 show typical experimental pressure distributions with measured and predicted separation point locations superimposed. Figure 4 shows results on a circular arc afterbody at Mach numbers of .25, .5 and .7. The control volume analysis accurately predicts the upstream movement of separation with increase in Mach number. Figure 5 gives similar results for an elliptical afterbody with three mean angles of 8°, 16° and 24°. This mean angle change affects the pressure distribution and control volume length, and in this manner changes the calculated separation point location. Again, the analysis accurately predicts the upstream movement of the separation point with increases in afterbody mean angle. Thus, the control volume separation calculation scheme appears to provide an accurate means for predicting the point of separation on a steep afterbody once the approach boundary-layer characteristics and true surface pressure distribution are known.

Recirculation Region Model

The typical flowfield in the vicinity of separation was shown in Fig. 1. The flow separates from the surface at some point, and flows over a low velocity recirculation region. Downstream at reattachment on the mounting sting, a pressure increase occurs due to the local flow curvature. A discriminating streamline is defined as a flow streamline at the edge of the separated bubble which has just enough kinetic energy to penetrate the downstream high pressure region and is the boundary between streamlines which continue downstream and those which recirculate. This discriminating streamline is used as the boundary of an effective body contour extending between the separation and reattachment points on the real body. The discriminating streamline is the boundary of the external flowfield and its shape primarily determines the surface pressures occurring between separation and reattachment points on an afterbody.

The pressure data of Ref. 1 typically show a plateau or constant pressure region which covers the majority of the model area between separation and reattachment. Since the recirculation region is composed of low energy, low velocity flow, the constant pressure in this region on the body surface must be nearly the same pressure that occurs on the discriminating streamline at a given x position. Thus, the external flowfield imposes its pressure distribution on the recirculation flow region. The question remaining is what shape the discriminating streamline must take to cause the constant pressure plateau regions which were consistently measured in the experiments. To determine this, the inviscid flow equations were examined in detail while noting that the separation region covers only a small radius change when compared to maximum radius of the afterbody. It was found from both analysis[6] and data[1] that a conical discriminating streamline will produce the constant plateau pressure region measured on separated afterbody models.

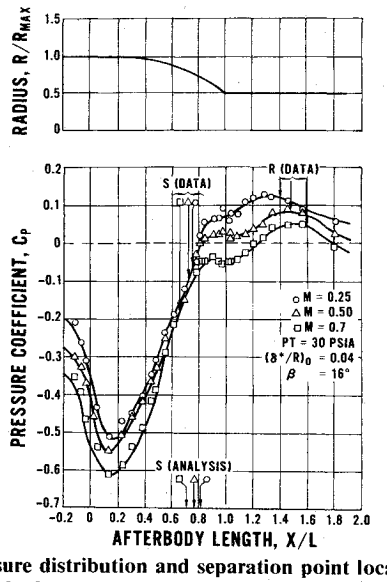

Fig. 4 Pressure distribution and separation point location on a circular arc afterbody.

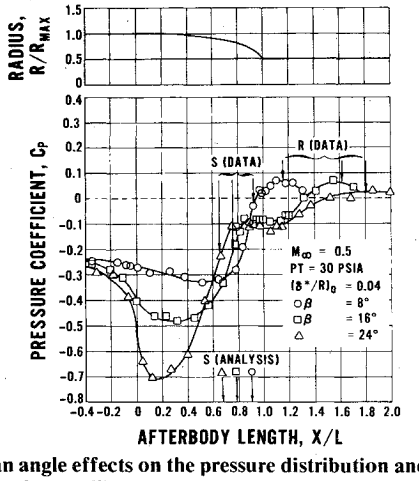

Fig. 5 Mean angle effects on the pressure distribution and separation point location for an elliptical afterbody.

To complete the flow calculation model of the recirculation region, a means must be developed to predict the angle between the discriminating streamline and body surface once the point of separation is determined. Figure 6 shows a control volume of the recirculation region in which the recirculating flow is assumed to be radial from the point of separation, and circular arc segments are taken as the inlet and discharge boundaries of the control surface. This coordinate system allows a smooth transition from the flow direction on the body surface to that on the discriminating streamline. The upper surface of the control volume is inclined at an angle ψ with the wall, and is a flow streamline so no mass flux passes through it. Applying the continuity and momentum equations, one obtains

$$x_{01}\int_0^{\psi}(\rho u)_1 \mathrm{d}\theta = x_{02}\int_0^{\psi}(\rho u)_2 \mathrm{d}\theta = 0 \tag{9}$$

and

$$\oint P\vec{n}\cdot \mathrm{d}\vec{S_x} + (\tau_{s\hat{n}})\Delta x_0 \cos\psi = J_{x2} - J_{x1} \tag{10}$$

where

$$J_x \equiv x_0 \int_0^{\psi} \rho u^2 (\cos\theta)\,\mathrm{d}\theta$$

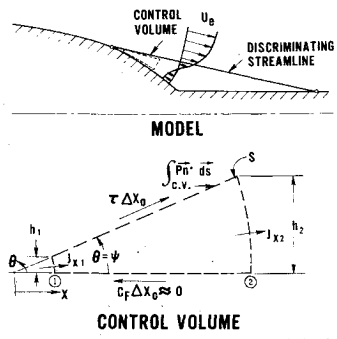

Fig. 6 Control volume of the recirculation region.

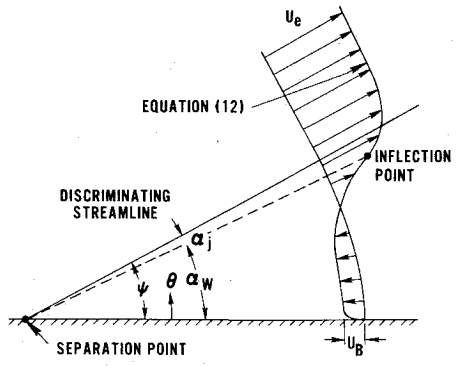

Fig. 7 Velocity profile in the recirculating flow region.

and

$$x_0 \equiv x(\theta = 0.0)$$

The large transverse pressure gradient regions near separation and reattachment are assumed to have only local effects [13] and are not included in this model. The pressure is nearly constant in the portion of the recirculation region included in the control volume so the first term drops out. Equation (10) thus becomes

$$\tau \Delta x_0 \cos\psi = J_{x2} - J_{x1} \tag{11}$$

In order to solve Eqs. (9) and (11), a velocity profile across the separation region has to be assumed so that the momentum flux as well as shear stress along the discriminating streamline can be estimated.

That portion of the recirculating flow occurring at nearly constant pressure is often termed a free shear layer. Korst et al. [14] Nash, [15] and Vasiliu [16] have used the similarity between the velocity distribution of a free shear and the velocity distribution of a jet flow in the analyses of problems involving such free shear layers associated with boundary-layer separation. The free shear layers encountered here will be treated in a like manner, i.e., a jet flow velocity distribution will be chosen to model the shear distribution and recirculating region.

The velocity across the mixed and reverse flow regions is therefore assumed to vary as an error function. The exact profile used is a modification of one developed by Korst and Chow, [17] which has been shown to accurately model nonisoenergetic turbulent mixing between two compressible streams at constant pressure

$$\frac{u}{u_e} = \left(1 + \frac{u_B}{u_e}\right)\left(\frac{1 + erf[\sigma(\theta - \alpha_w)]}{2}\right) - \frac{u_B}{u_e} \tag{12}$$

where

$$\sigma \equiv 12(1 + .23M_s)$$

$$\eta \equiv \frac{\sigma y}{x} = \sigma(\theta - \alpha_w)$$

This velocity profile is shown in Fig. 7. u_B is an assumed slip velocity at the wall. This apparent violation of the no slip wall condition is not a major drawback of the profile since it has been shown by both Sawyer, [18] and Jones, Foster, and Mitchell [19] that the reverse flow drops rapidly from a maximum velocity to zero in a region very close to the wall as shown. Again, $\theta = \psi$ is the angle of inclination between the discriminating streamline and afterbody surface. From the geometry in the figure it is clear that

$$\psi = \alpha_j + \alpha_w \tag{13}$$

Relations for the turbulent shearing stress along the discriminating streamline and the angle α_j, both obtained by Korst and Chow [17] are

$$F \equiv \tau\, \Delta x = \frac{(.148 - .036\, M_s)}{\sigma} \rho u_e^2 \Delta x_0 \tag{14}$$

$$\alpha_j = \frac{(.209 + .052\, M_s)}{\sigma} \tag{15}$$

Equations (9), and (11-14) can be combined to give the following three governing equations

$$\psi = \frac{(.209 + .052\, M_s)}{\sigma} + \alpha_w \tag{16}$$

$$\int \frac{\rho}{\rho_e}\left\{\left(1 + \frac{u_B}{u_e}\right)\left[\frac{1 + \mathrm{erf}(\sigma[\theta - \alpha_w])}{2}\right] - \frac{u_B}{u_e}\right\} d\theta = 0 \tag{17}$$

$$\int_0^{\psi} \frac{\rho}{\rho_e}\left\{\left(1 + \frac{u_B}{u_e}\right)^2\left[\frac{1 + \mathrm{erf}(\sigma[\theta - \alpha_w])}{2}\right]^2 - 2\left(\frac{u_B}{u_e}\right)\left(1 + \frac{u_B}{u_e}\right)\left[\frac{1 + \mathrm{erf}(\sigma[i - q_w])}{2}\right] + \left(\frac{u_B}{u_e}\right)^2\right\} \cos\theta\, d\theta = \frac{(.148 - .036\, M_s)}{\sigma} \cos\psi \tag{18}$$

Equations (16), (17), and (18) comprise a proper set of three equations with three unknowns: ψ, α_w and u_B. Given a Mach number at separation, these equations can be iteratively solved for the separation angle ψ.

Figure 8 presents a comparison of measured and predicted separation angles as a function of Mach number. The solid line in this figure is the calculated result from a solution of the equation above. The symbols represent the results from the 33 test runs. [6] The data scatter around the predicted results could be due to either inaccuracies in the experimental flow visualization technique, analytical model, or both. With this in mind, the overall agreement between the analysis and data is quite good. The separation angle decreases with increasing Mach number, starting off at an angle greater than 14° for the incompressible case, and ending up roughly 11° at Mach one.

Overall Separation Analysis

Given an accurate separation point predictor and a model of the recirculation region, a complete analysis of the separated flow over an afterbody can now be developed. The model is based on an iterative matching between four components: an inviscid flowfield calculation; an attached boundary-layer calculation; the control volume separation point prediction; and the separated flowfield model. In this iterative approach, one first assumes no separation on the afterbody

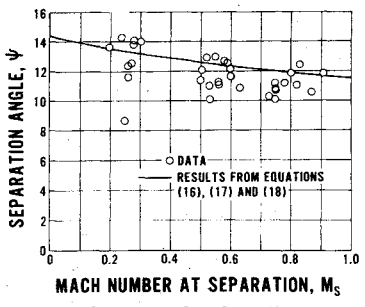

Fig. 8 A comparison of measured and predicted separation angles.

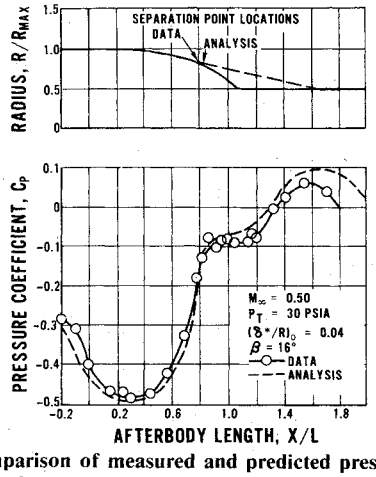

Fig. 9 A comparison of measured and predicted pressures over an elliptical afterbody.

and then the inviscid flowfield and corresponding pressure distribution on the body are calculated. Next, a momentum integral, turbulent boundary-layer program is used to calculate the boundary-layer development on the body prior to separation. The separation point is then determined by the control volume calculation. Finally, a recirculating flow region is defined by a straight discriminating streamline between the external flow and the recirculating flow as shown in Fig. 2. This discriminating streamline acts as the boundary of a fictitious body extending between the separation and reattachment points on the real body. The inviscid flowfield is then recomputed for the flow over the modified afterbody shape. This gives a new external pressure field which is used with the boundary layer program and separation prediction criterion to determine a new separation point and aerodynamic lines for the afterbody, and so on, continuing the iteration until the solution converges. This separation point prediction and the separated flow model could both be combined in a like manner with any inviscid flowfield attached boundary calculation for predicting, a priori, the effects of separation on afterbody pressures and drags.

The results that follow were calculated using a potential flow analysis for the inviscid flow which uses a distribution of sources and sinks over the body surface to satisfy the surface boundary conditions as presented by Smith and Pierce.[20] The boundaries due to wind tunnel walls were also included so that blockage effects were properly simulated in predicting the pressure field for comparison with experimental results. The attached boundary-layer calculation used was based on a momentum intergral approach developed by Reshotko and Tucker.[2]

Figure 9 presents a comparison of measured and calculated pressure distributions over a separated, elliptical afterbody at $M_\infty = .50$. The minimum pressure and recompression are all predicted quite well by the iterative procedure. The corresponding calculated and measured drag variations with mean angle

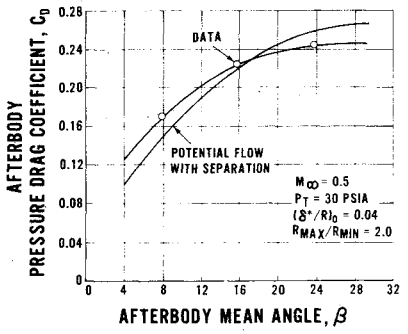

Fig. 10 A comparison of measured and predicted drag coefficients on elliptical afterbodies.

for an elliptical afterbody are shown in Fig. 10 in terms of drag coefficients, C_D, based on maximum afterbody area. A drag variation with mean angle is calculated that agrees quite well with the data in both magnitude and shape. It would then appear that this is a viable procedure to predict afterbody drag in the absence of experimental data.

Conclusions

The results of this analytical program suggest the following conclusions about separation over an axisymmetric afterbody: 1) An axisymmetric control volume analysis using a realistic separation velocity profile can be used to accurately predict the separation point on an afterbody. 2) The separated region can be modeled fairly well by a conical dividing streamline surface between the points of separation reattachment. The inviscid pressure distribution over the body, including this dividing streamline, seems to be a good first order approximation to the actual separation pressure field. 3) Assuming the shear distribution in the free shear layer and recirculation region to be the same as in a constant pressure jet, the separation angle for the discriminating streamline can be predicted quite accurately as a function of separation Mach number. 4) An iteration scheme involving an inviscid flow calculation, an attached boundary layer calculation, and a conical discriminating streamline to approximate the recirculation region, will converge and accurately predict the separated afterbody pressure distribution and drag without recourse to the experimental data.

References

[1] Presz, W. and Pitkin, E., "Flow Separation Over Axisymmetric Afterbody Models," *Journal of Aircraft*, Vol. 11, Nov. 1974, pp. 677-682.

[2] Reshotko, E. and Tucker, M., "Approximate Calculation of the Compressible Turbulent Boundary Layer with Heat Transfer and Arbitrary Pressure Gradient," NASA TN-4154, 1957.

[3] Goldschmied, F. R., "An Approach to Turbulent Incompressible Separation Under Adverse Pressure Gradients," *Journal of Aircraft*, Vol. 2, March-April 1965, pp. 108-115.

[4] Page, R. H., "A Theory for Incipient Separation," *Development in Mechanics*, Vol. 1, Plenum Press, N.Y., 1961, pp. 563-577.

[5] Stratford, B. S., "The Prediction of the Turbulent Boundary Layer," *Journal of Fluid Mechanics*, Vol. 5, Jan. 1959, pp. 1-16.

[6] Presz, W. M., Jr., "Turbulent Boundary Layer Separation on Axisymmetric Afterbodies," Ph.D. thesis, 1974, School of Engineering, Univ. of Connecticut, Stoors, Conn.

[7] Tyler, R. D. and Shapiro, A. H., "Pressure Rise Required for Separation in Interaction Between a Turbulent Boundary Layer and Shock Wave," *Journal of Aeronautical Science*, Vol. 20, 1953, pp. 858-860.

[8] Presz, W. and Mathews, D., "Control Volume Analysis of Afterbody Separation," Pratt and Whitney Aircraft, E. Hartford, Conn., SMR 4887, Aug. 1973.

[9] Green, J. E., "The Prediction of Turbulent Boundary Layer Development in Compressible Flow," *Journal of Fluid Mechanics*, Vol. 31, April 1968, pp. 753-778.

[10]Coles, D., "The Law of the Wake in Turbulent Boundary Layer," *Journal of Fluid Mechanics*, Vol. 1, July 1956, pp. 191-226.

[11]Kline, S. J., et al., "Computation of Turbulent Boundary Layers," Proceedings of the AFOSR – IFP-Stanford Conference, Vols. 1 and 2, Stanford University Press, Stanford, Calif., 1968.

[12]Mathews, D. C., Childs, M. E. and Paynter, G. C., "Use of Coles' Universal Wall Function for Compressible Turbulent Boundary Layers," *Journal of Aircraft*, Vol. 7, March 1970, pp. 137-140.

[13]Kuhn, G. and Nielsen, J., "An Analytical Method for Calculating Turbulent Separated Flows Due to Adverse Gradients," Project Squid, Purdue University, Lafayette, Ind., TRNEAR-1-PU, 1971.

[14]Korst, H. H., Page, R. H. and Childs, M. E., "Compressible Twoo-Dimensional Jet Mixing at Constant Pressure," Mech. Eng. Dept., University of Illinois, Urbana, Ill, TN392-1, 1954.

[15]Nash, H. F., "An Analysis of Two-Dimensional Turbulent Base Flow, Including the Effect of the Approaching Boundary Layer," Aeronautical Research Council, National Physical Laboratory, Teddington, England, R&M No. 3344, 1960.

[16]Vasiliu, J., "Pressure Distribution in Regions of Step Induced Turbulent Separation," *Journal of Aerospace Science*, Vol. 29, 1962, p. 596.

[17]Korst, H. H. and Chow, W. L., "Non-Isoenergentic Turbulent Jet Mixing Between Two Compressible Stream at Constant Pressure" NASA CR-149, 1966.

[18]Sawyer, R. A., "The Flow Due to a Two-Dimensional Jet Issuing Parallel to a Flat Plate," *Journal of Fluid Mechanics*, Vol. 9, Dec. 1960, pp. 543-561.

[19]Jones, N. S., Foster, K. and Mitchell, D. G., "A Method of Calculating The Wall Pressure Distribution in a Turbulent Reattachment Bubble," Second Cranfield FluiDynamics Conf., Paper A-3, 1967.

[20]Smith, A. M. O. and Pierce, J., "Exact Solution of the Nuemann Problem; Calculation of Non-Circulatory Plane and Axial Symmetry Flow About or Within Arbitrary Boundaries," *Proceedings of the Third U.S. National Congress of Applied Mechanics*, Vol. 2, Brown University, Providence, R.I., 1968, pp. 807-815.